Journal of the European Ceramic Society **12** (1993) 177–184

Parabolic–Non-Parabolic Oxidation Kinetics of Si_3N_4

Jeanette Persson, Per-Olov Käll & Mats Nygren

Department of Inorganic Chemistry, Arrhenius Laboratory, Stockholm University, S-106 91 Stockholm, Sweden

(Received 10 December 1992; revised version received 24 February 1993; accepted 19 March 1993)

Abstract

The isothermal oxidation behaviour of Si_3N_4, HIP sintered without additives, has been investigated thermogravimetrically in the temperature range 1250–1500°C. The formed oxide scales were found to be partly crystalline, and the obtained weight gain curves followed the parabolic rate law after a certain time, t_o, but not during the entire oxidation experiment. In the time interval $t < t_o$ the curves have been interpreted with the rate law $\Delta w/A_o = a \arctan \sqrt{bt} + c\sqrt{t} + d$, which is developed with the assumption that the cross-section area available for oxygen diffusion decreases during the experiment, due to a crystallization process and to formation of nitrogen bubbles within the oxide scale. The rate constants, K_p were calculated from the constants in the arctan function, and the activation energy could be determined to be 310 ± 25 kJ/mol. The oxygen diffusion rates found are in fair agreement with those obtained for amorphous silica.

Das isothermische Oxidationsverhalten von ohne Zusätze HIP gesintertem Si_3N_4 wurde thermogravitometrisch im Temperaturbereich zwischen 1250 und 1500°C untersucht. Die sich bildenden Oxidationsschichten waren teilweise kristallin, und die sich ergebenden Gewichtszunahmekurven folgten nach einiger Zeit, t_o, einem parabolischen Ratengesetz. Allerdings galt diese Gesetzmäßigkeit nicht für die gesamte Dauer des Experiments. Im Zeitintervall $t < t_o$ wurden die Kurven durch das Ratengesetz $\Delta w/A_o = a \arctan \sqrt{bt} + c\sqrt{t} + d$ beschrieben, das von der Annahme ausgeht, daß die Querschnittsfläche für die Sauerstoffdiffusion während des Experiments aufgrund eines Kristallisationsprozesses und der Bildung von Stickstoffblasen innerhalb der Oxidationsschicht abnimmt. Die Ratenkonstante, K_p, wurde aus den Konstanten in der arctan-Funktion bestimmt. Die Aktivierungsenergie ergab sich zu 310 ± 25 kJ/mol. Die gefundenen Sauerstoffdiffusionsraten sind in guter Übereinstimmung mit den Raten, an amorphem Siliziumoxid, wurden.

Le comportement à l'oxydation isotherme du Si_3N_4, fritté par HIP sans aides au frittage, a été étudié par thermogravimétrie dans l'intervalle de température de 1250 à 1500°C. Les couches oxydées se sont révélées partiellement cristallines, et les courbes de gain de poids obtenues suivent une loi parabolique après un certain temps, t_o, mais pas pendant l'entièreté de l'essai d'oxydation. Dans l'intervalle de temps $t < t_o$, les courbes ont été interprétées au départ d'une loi cinétique. $\Delta w/A_o = a \arctan \sqrt{bt} + c\sqrt{t} + d$, que l'on a développée en supposant que l'aire de la section disponible pour la diffusion de l'oxygène diminue pendant l'expérience en raison d'un processus de cristallisation et de la formation de bulles d'azote au sein de la couche oxydée. Les constantes cinétiques, K_p, ont été calculées au départ des constantes de la fonction arctangente et l'énergie d'activation déterminée est de 310 ± 25 kJ/mole. Les vitesses de diffusion d'oxygène sont en accord avec celles obtenues pour la silice amorphe.

Introduction

Most Si_3N_4-based ceramic materials are prepared with addition of a sintering aid to simplify the densification. The oxidation resistance of these materials is found to depend on the type and amount of intergranular phase formed during densification. The oxidation rate is found to increase with increasing amount and decreasing viscosity of the intergranular glassy phase formed. It is generally believed that the diffusion of the additive ions from the matrix into the oxide scale controls the oxidation rate.[1–5]

For materials prepared without a sintering aid the

Journal of the European Ceramic Society 0955-2219/93/$6.00

oxidation rate is found to depend on the oxygen partial pressure but not on the nitrogen partial pressure.[6] This implies that the oxidation rate is controlled by diffusion of oxygen through the oxide scale. Oxidation studies of SiC at different oxygen partial pressures have shown that: (i) the diffusing species is O_2 at temperatures below 1400°C[7,8] and O^{2-} above 1400°C;[9] (ii) the activation energy of diffusion is higher for O^{2-} ions ($\approx$300 kJ/mol) than that for O_2 (120 kJ/mol). Compared to SiC, lower K_p-values and higher activation energies are found by oxidation studies of Si_3N_4 (300–400 kJ/mol) even at $T < 1400$°C. It has been suggested that the lower rate constants and the higher activation energy are due to the presence of an Si_2N_2O layer between the SiO_2 oxide scale and the Si_3N_4 matrix and that the oxygen diffusion rate through this Si_2N_2O layer is lower than through SiO_2.[6] It has also been suggested that the nitrogen reaction products might impede the reaction kinetics, resulting in higher E_a-values.[10]

The oxidation of Si_3N_4-based materials and other materials (e.g. Si and SiC) that form a silica surface layer upon oxidation is controlled by diffusion and is generally interpreted with the parabolic rate law.

$$(\Delta w/A_o)^2 = K_p t + B \qquad (1)$$

where $\Delta w/A_o$ is the weight gain per surface area, K_p the parabolic rate constant t the time and B an additive constant.

Deviations from the parabolic rate law, especially at high temperatures, have, however, been reported both for materials prepared with sintering aids[11–13] and without.[9,14,15] These deviations have been attributed to crystallization and to formation of N_2-bubbles in the oxide scale. The oxidation has in these cases been reported to follow either a logarithmic rate law,[11,12,14] to obey the Avrami equation[15] or has been described as being composed of two parabolic parts.[9] In the latter case, an amorphous oxide scale is formed during the first part of the oxidation, while during the second part the scale is crystalline. The first part exhibits a lower activation energy than the second.

Previous oxidation studies of Si_2N_2O, performed by us, have shown that deviations from the parabolic rate law occurred at temperatures above 1300°C.[16] The obtained oxidation curves could be interpreted with a new rate law, which reads $\Delta w/A_o = a \arctan \sqrt{bt} + c\sqrt{t}$. This rate law is derived by incorporation of a function $A(t)$, which describes the decrease of the cross-section area of the amorphous phase available for oxygen diffusion, in the parabolic rate law, as will be briefly outlined below. The decrease of the area might be a result of a crystallization process and of formation of nitrogen bubbles and cracks within the oxide scale. The model is based on the assumption that the oxygen diffusion through the crystalline phase is negligible compared to the oxygen diffusion through the amorphous phase.

This article concerns the oxidation of Si_3N_4: to what extent the oxidation curves can be consistently interpreted with this new rate law.

Experimental

Pieces of β-Si_3N_4 ceramic were prepared from α-Si_3N_4 powder (UBE, grade SN10E). The cold-pressed samples were glass encapsulated and hot isostatically pressed (HIP) at 1950°C for 2 h at an argon pressure of 200 MPa. The X-ray powder pattern of the Si_3N_4 ceramic showed that a single phase β-Si_3N_4 material ($a = 7{\cdot}601$ Å, $c = 2{\cdot}907$ Å) had been obtained, and the density was determined to be 99·5% of the theoretical density, using Archimedes' principle.

Before oxidation, the ceramic body was cut into pieces of approximate size $15 \times 15 \times 1$ mm^3. The pieces were carefully polished with diamond grains down to < 1 μm, and a small hole was drilled in each piece. Finally the samples were cleaned in boiling toluene and ultrasonically cleaned in acetone.

The oxidation experiments were performed in a TG unit (SETARAM TAG 24). The TG unit has two symmetrical furnaces, one used for the oxidation of the sample and the other for an inert reference. By regulation of the gas flow through the two furnaces the drift of the baseline for 20 h could be kept within ± 5 μg. This configuration makes it possible to record very accurate oxidation data. The oxidation was performed isothermally for 20 h at different temperatures ranging from 1250 to 1500°C in flowing oxygen. The samples were heated up to the temperature chosen for the isothermal oxidation experiment with a heating rate of 100 K/min in oxygen.

The oxide surfaces and the cross-sections of the oxide scales were studied in a scanning electron microscope (SEM), JEOL 880, equipped with an energy dispersive spectrometer (EDS), Link AN 10000. The crystalline phases present in the oxide scales were identified by their diffractograms obtained in an X-ray powder diffractometer (STOE STADI) operated in reflection mode with Cu $K\alpha_1$ radiation.

Results and Discussion

Oxidation curves

The weight gain curves obtained in the temperature region 1250–1500°C are shown in Fig. 1. The final weight gains are moderate, indicating formation of a coherent oxide layer, except for the one obtained at

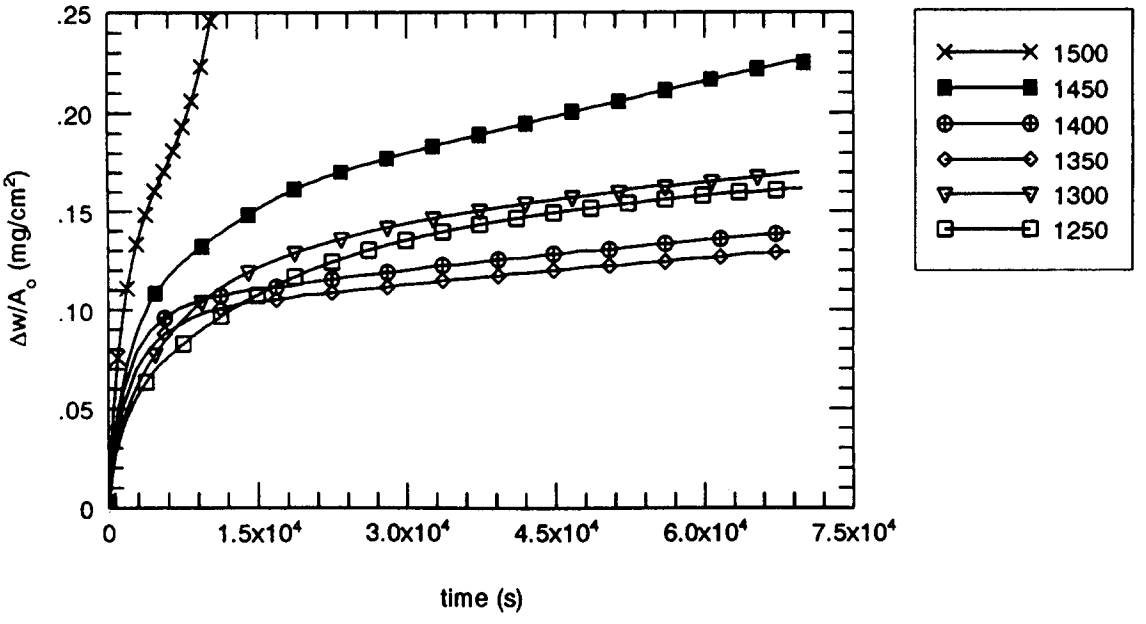

Fig. 1. The weight gain plotted versus time for the oxidation of Si_3N_4 in the temperature interval 1250–1500°C in oxygen.

1500°C, where the weight gain increases very rapidly. The final weight gains do not, however, strictly increase with increasing temperature. Oxidation curves obtained at the same temperature are also different. This is illustrated in Fig. 2, where duplicate oxidation curves obtained both at 1250 and 1400°C are given. The final weight gains of the two curves recorded at the same temperature differ considerably and there is also an overlap of the final weight gain of the curves obtained at 1250 and 1400°C.

The shapes of the oxidation curves are also different. This is more clearly seen by plotting the squared weight gain versus time [Fig. 3(a), (b)]. The curves are convex at the beginning of the oxidation but become linear after some time, except the one obtained at 1250°C, which is convex during the

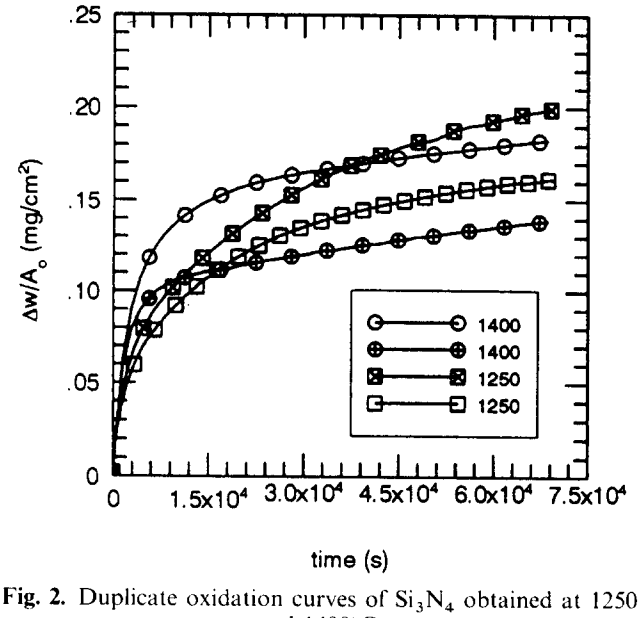

Fig. 2. Duplicate oxidation curves of Si_3N_4 obtained at 1250 and 1400°C.

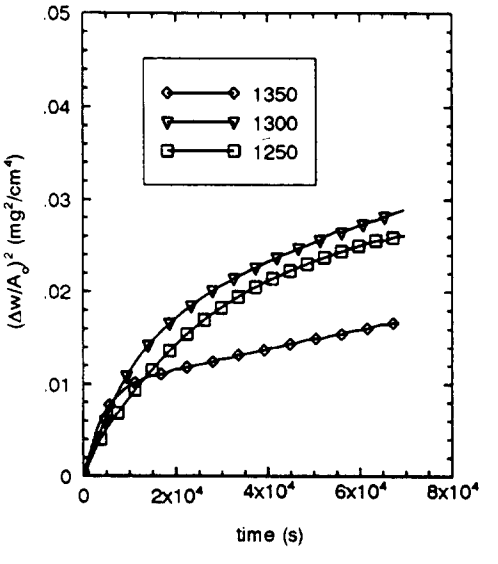

(a)

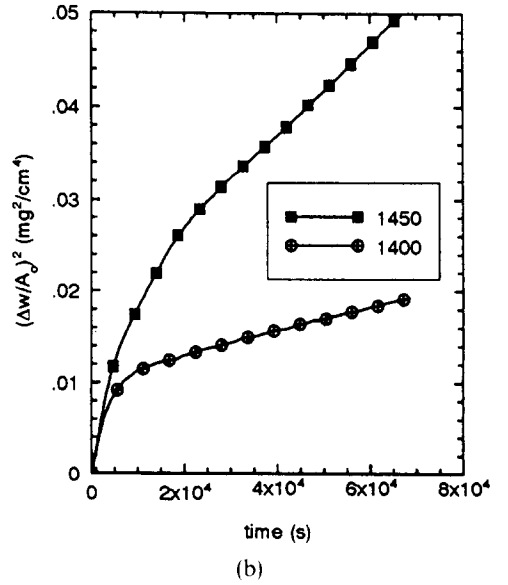

(b)

Fig. 3. (a), (b) A parabolic plot of the weight gain of Si_3N_4 during oxidation in the temperature range 1250–1500°C.

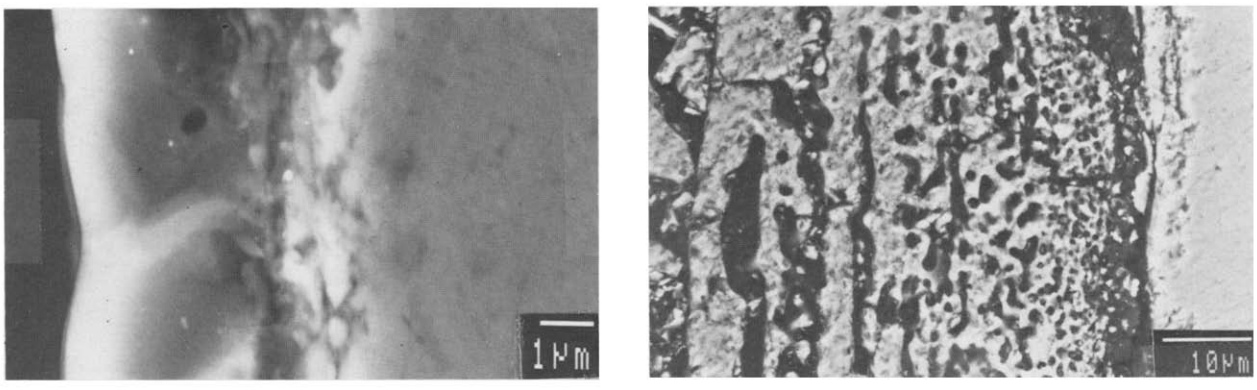

(a) (b)

Fig. 4. Micrographs of the cross-sections of: (a) the dense oxide scale formed at 1400°C; (b) porous oxide scale formed at 1500°C.

entire time. The convexity of these curves shows that the oxidation process cannot solely be explained by the parabolic rate-law.

Oxide scale

The cross-sections of the oxide scales formed at 1400 and 1500°C are shown in Fig. 4. At 1400°C, the scale is dense but contains small nitrogen bubbles. At 1500°C, however, the scale has a porous structure, which is consistent with the observed breakaway oxidation behaviour. The X-ray diffraction patterns of the oxidized surfaces showed that the oxide scales contained tridymite ($T < 1500$°C), α-cristobalite and very small amounts of Si_2N_2O. Tridymite dominates at lower temperatures and α-cristobalite at higher. These crystalline phases are also observed in the SEM micrographs of the oxidized surfaces, shown in Fig. 5(a)–(d). The oxide scales obtained at $T < 1500$°C are coherent, the crystals are surrounded by a liquid film and only a few small holes, formed due to the nitrogen evolution, are observed. At 1500°C, however, cavities or channels are found between the grains, implying that the amorphous phase does not fill up the space between the crystals to give a coherent oxide scale [see Figs 4(b) and 5(d)].

Oxidation kinetics

The parabolic rate law [eqn (1)] could not be fitted to the oxidation curves from the beginning to the end of the experiment at any temperature. But the

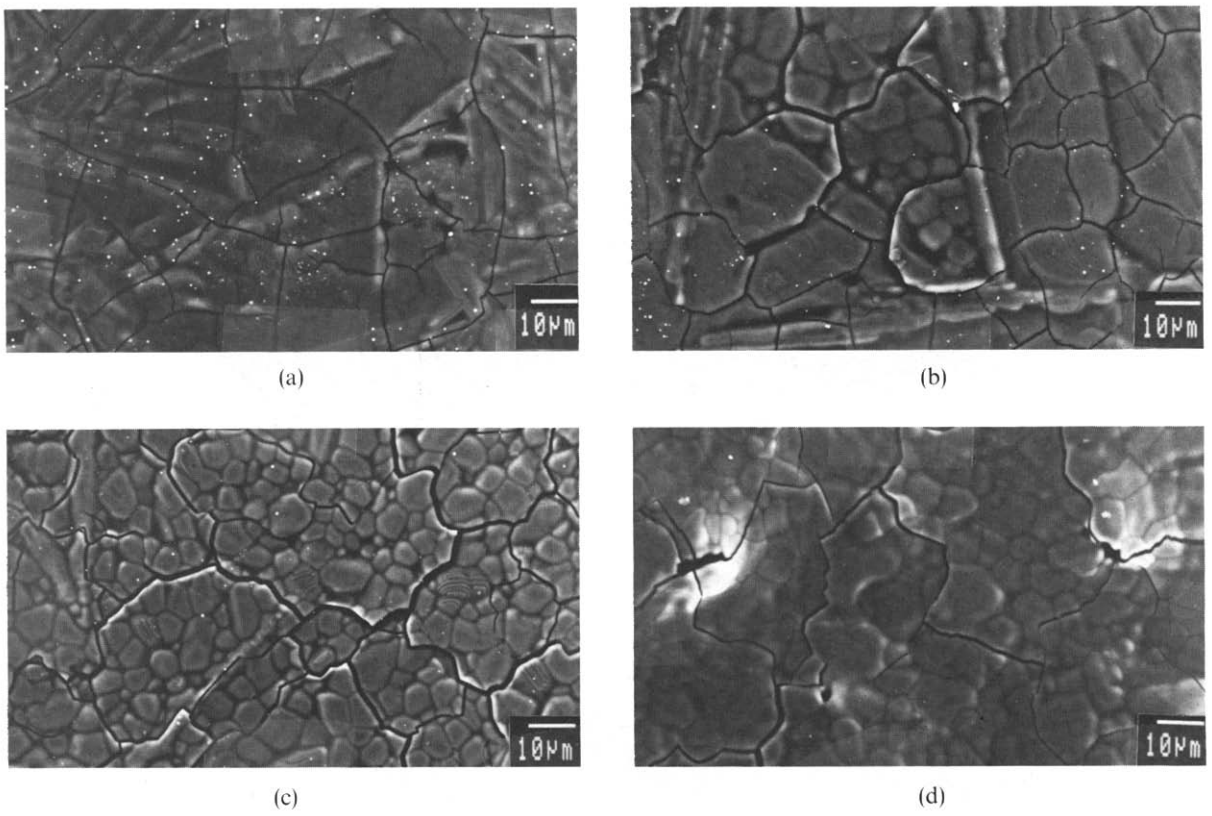

(a) (b)

(c) (d)

Fig. 5. Micrographs of the oxide surface formed at: (a) 1250°C; (b) 1350°C; (c) 1400°C and (d) 1500°C. The micrographs (a), (b) and (c) are taken in BSE mode (back scattered electrons) while (d) is taken in SE mode (secondary electrons).

convex curvature of the squared weight gain curves (see Fig. 3) and the presence of crystals in the oxide scale indicate that the new rate law might be applicable. This rate law is derived with the assumption that the weight gain is mainly a result of oxygen diffusing through a decreasing cross-section area of the amorphous phase due to crystallization in the oxide scale.

We have previously[16] derived a function, $A(t)$, which is based on experimental observations and expressed as

$$A(t) = A_o \frac{(1 + (f\beta - t_o^{-1})t)}{(1 + (\beta - t_o^{-1})t)} \tag{2}$$

where A_o is the initial surface area, β is the rate constant for the decrease of the area, f is the fraction of the original area, A_o, and t_o is the time at which a steady state is reached, i.e. after which the decrease of the area is negligible. By substituting the area function, $A(t)$ for A_o in

$$\mathrm{d}\,\Delta w = \frac{A_o\sqrt{K_p}}{2\sqrt{t}}\,\mathrm{d}t \tag{3}$$

and integrating the new rate law is obtained, which reads

$$\frac{\Delta w}{A_o} = a \arctan\sqrt{bt} + c\sqrt{t} \tag{4}$$

$$a = \frac{\beta\sqrt{K_p}(1-f)}{b^{3/2}} \qquad b = \beta - t_o^{-1}$$

$$c = \frac{\sqrt{K_p}(f\beta - t_o^{-1})}{b}$$

$$K_p = (a\sqrt{b} + c)^2 \qquad f = \frac{\dfrac{a\sqrt{b}}{bt_o + 1} + c}{a\sqrt{b} + c}$$

This equation is valid for $t < t_o$. If t_o is reached within the experimental time, a parabolic behaviour is observed for $t > t_o$, as $A(t)$ now is constant. This parabolic function is expressed as

$$(\Delta w/A_o)^2 = K_p^o + B_o \tag{5}$$

where K_p^o is an 'apparent' rate constant and B_o an additive constant >0. As the derivates of the arctan and the parabolic functions are equal at $t = t_o$, the relation between K_p and K_p^o becomes

$$K_p = \frac{K_p^o t_o}{f^2\left(t_o + \dfrac{B_0}{K_p^o}\right)} \tag{6}$$

All the recorded oxidation curves could be described by the new rate law [eqn. (4)] in combination with the parabolic rate law [eqn. (5)]. The oxidation curve obtained at 1250°C followed an arctan function

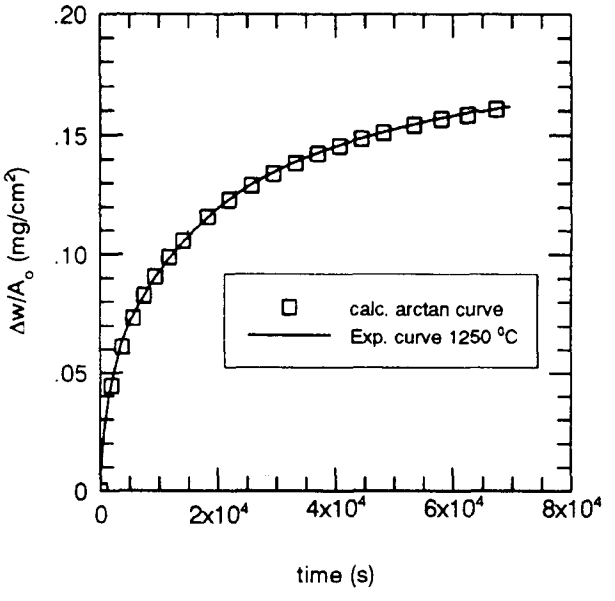

Fig. 6. The experimental and calculated weight gain curves for the oxidation of Si_3N_4 at 1250 C.

during the entire oxidation time, as shown in Fig. 6, and the curves obtained at higher temperatures could all be fitted by the arctan function during the first part of the experiment and by the parabolic rate law for $t > t_o$. An example of this oxidation behaviour is shown in Fig. 7, where the experimental curve obtained at 1400°C and the calculated curves are shown. The t_o value was in this case determined to be 33 000 s.

Examining the first part of the oxidation curves, it was found that they did not follow the arctan function until after a couple of hundred seconds, which is shown in Fig. 8. The first part was found to be paralinear. During this initial part the nitrogen bubbles break through the oxide layer and thereby

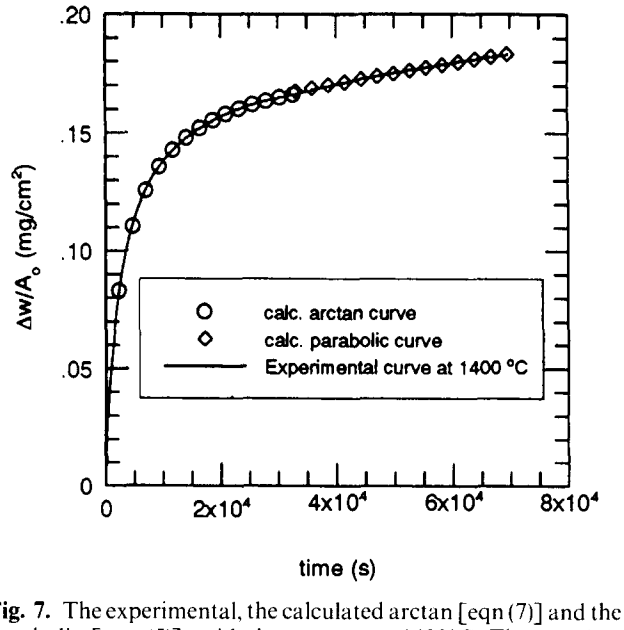

Fig. 7. The experimental, the calculated arctan [eqn (7)] and the parabolic [eqn (5)] oxidation curves at 1400°C. The t_o value, where the arctan functions is followed by the parabolic function is determined to be 33 000 s.

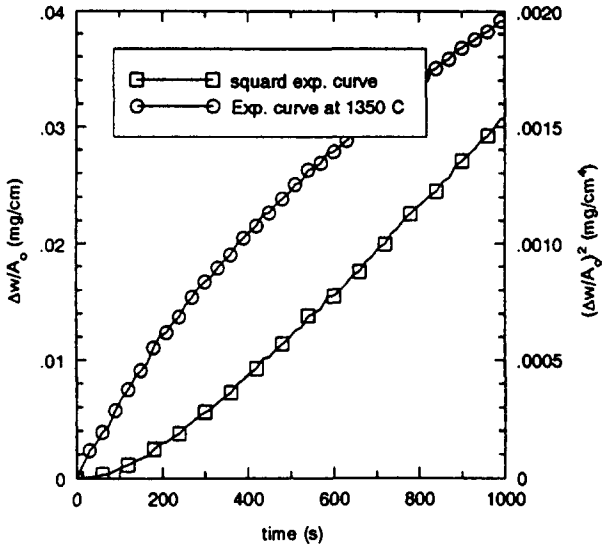

Fig. 8. The weight gain (left axis) and the squared weight gain (right axis) plotted versus time for the first 1000 s of the oxidation of Si_3N_4 at 1350 C. The squared weight gain curve has a concave curvature during the first 600 s before it turns convex. It is also possible to observe the paralinear behaviour in the beginning of the experimental curve.

expose unreacted Si_3N_4 to the oxidizing environment. This process proceeds until a sufficiently thick oxide scale is formed. Accordingly, this first part of the oxidation curve is not included in the least-squares refinement of the arctan function to fit the experimental data. The occurrence of an initial paralinear part also implies that the origin of the arctan function is different from the experimental one. In order to account for this, a constant d is introduced to eqn (4), which then reads

$$\Delta w/A_o = a \arctan \sqrt{bt} + c\sqrt{t} + d \qquad (7)$$

The calculated constants according to eqn (7), K_p, K_p^o, t_o, f and β are given in Table 1. The final weight gains of the duplicate oxidation experiments at the same temperature were found not to coincide (see Fig. 2) but similar K_p values were, anyhow, obtained. This shows that the final weight gain obtained also depends on the calculated f value, i.e. on the evolution of the microstructure of the oxide scale. The K_p values are found to increase with increasing temperature, although the final weight gains do not strictly increase with temperature. This coincides with the observation that the f values decrease with increasing temperature. It can also be noted that the K_p values are calculated using the constants of the fitted arctan function for $t < t_o$ and it can be observed in Fig. 1 and in Fig. 2 that the weight gains increase with increasing temperature during the first 5000 s. The rate of the decrease of the cross-section area, β, is found to increase with temperature as expected.

Table 1. The calculated oxidation parameters for Si_3N_4 according to eqns (7), (4), (5), (6), (8) and (9)

T (°C)	Δw (*after 20 h*) (mg/cm^2)	a (mg/cm^2)	b 10^{-4} (*per s*)	c 10^{-4} ($mg/cm^2\ per\ s^{1/2}$)	d 10^{-2} (mg/cm^2)	K_p 10^{-6} ($mg^2/cm^4\ per\ s^2$)
1 250	0·16	0·197	0·371	−1·41	−0·022 8	1·12
1 250	0·20	0·150	0·401	1·59	0·425	1·23
1 300	0·17	0·165	0·865	−0·796	−0·962	2·12
1 300	0·27	1·48 10^{-3}[a]	−7·50 10^{-5}[a]	—	−0·439	2·19
1 350	0·13	0·125	4·25	−1·59	−2·53	5·88
1 400	0·18	0·173	2·94	−1·12	−3·12	8·14
1 400	0·14	0·126	8·02	−0·935	−4·04	12·2
1 450	0·23	0·111	5·82	3·78	−3·31	9·37
1 450	0·19	0·103	16·7	0·571	−4·20	18·3
1 500	2·8	0·188[b]	21·6[b]	9·03[b]	−117[b]	93·3[b]
1 500	2·2	0·138[b]	9·37[b]	9·00[b]	−55·3[b]	26·1[b]

[a] a_1 and b_1 in eqn (8).
[b] Calculated from the data obtained during the first 7000 s.

T (°C)	K_p^o 10^{-7} ($mg^2/cm^4\ per\ s^1$)	B_o 10^{-2} (mg^2/cm^4)	t_o (*s*)	f	β 10^{-4} (*per s*)	α 10^{-12} (cm^2/s)
1 250	—	—	> 70 000	0·18	0·471	4·22
1 250	—	—	> 70 000	0·37	0·500	4·64
1 300	1·74	1·68	41 011	0·12	1·12	8·00
1 300	4·15	3·83	50 000	0·24	0·20	7·72
1 350	1·04	0·964	18 527	0·05	4·79	22·2
1 400	1·50	2·31	33 186	0·06	3·24	30·7
1 400	1·28	1·06	17 169	0·04	8·61	46·0
1 450	4·78	1·75	38 574	0·16	6·08	35·4
1 450	—	—	—	—	17·2	69·2
1 500	—	—	—	—	—	352
1 500	—	—	—	—	—	98·5

The calculated parameters for the oxidation curves obtained at 1450°C and especially for those obtained at 1500°C are very imprecise, because these curves exhibit a more or less pronounced breakaway oxidation behaviour. This also implies that K_p^o and t_o-values could not be determined for these curves. The K_p values given in Table 1 were calculated by fitting the arctan function to the very first part of the experimental curve, where this function still seemed to be valid.

One of the curves obtained at 1300°C could not be fitted by the arctan function, but by the function

$$\Delta w/A_o = y = a_1\sqrt{t} + b_1 t^{1.5} + d \qquad (8)$$

This function is obtained by integration of eqn (3) with $\beta = 1/t_o$ in eqn (2). K_p and f can be calculated from $(a_1)^2$ and $(3b_1/\beta a_1)+1$, respectively.

The temperature dependence of the parabolic rate constants for Si_3N_4 is shown in an Arrhenius plot in Fig. 9, and they are compared with those previously determined for Si_2N_2O.[16] The parabolic rate constants calculated for Si_3N_4 are about one magnitude higher than those for Si_2N_2O. The activation energy was determined to be 310 ± 25 kJ/mol, which is about the same as determined for Si_2N_2O (245 kJ/mol). The rate constants at 1450 and 1500°C are not used in the calculation of the activation energy for Si_3N_4, but they do fit rather well with the extrapolated line in Fig. 9. The 'apparent' parabolic rate constants, K_p^o, are also given in the figure. The K_p^o values do, however, not show a linear dependence on the temperature in the Arrhenius plot.

Oxidation curves with a mixed arctan and parabolic oxidation behaviour were found at $T > 1250$°C for Si_3N_4 but at $T \geq 1500$°C in the case of Si_2N_2O. That is, the change from a pure arctan kinetic to a mixed arctan and parabolic kinetic occurs at a lower temperature for Si_3N_4 than for Si_2N_2O. Accordingly, we observe that a steady state occurs at a later stage of the oxidation experiment for Si_3N_4 ($t_o \approx 5$–10 h) than for Si_2N_2O ($t_o \approx 3$ h).

Because the nitrogen concentration is not the same in Si_3N_4 and Si_2N_2O ceramics, the same weight gain corresponds to a somewhat different thickness of the oxide scale. If α is taken as the growth rate of the oxide scale, which in turn is proportional to the oxygen diffusion coefficient, then

$$\alpha = \frac{K_p}{\rho_e^2} \qquad (9)$$

where ρ_e is an 'effective density' of the oxide scale, which correlates the weight gain with the thickness of the oxide scale. It is calculated as

$$\rho_e = \frac{(M_{O_2} n_{O_2} - M_{N_2} n_{N_2})}{\sum M_i n_i / \rho_i} \qquad (10)$$

where M_{O_2} and M_{N_2} are the molecular weights of oxygen and nitrogen, n_{O_2} and n_{N_2} are the amounts of oxygen absorbed and nitrogen released, M_i and n_i denote the molecular weight and the amount of oxide i formed, and ρ_i the densities of the oxides in the scale (here SiO_2).

The α-values for Si_3N_4 are compared in Fig. 10 with previously reported α-values determined from oxidation studies of Si_3N_4, Si_2N_2O, single crystals of Si and with the oxygen diffusion coefficients in amorphous silica determined by isotope exchange method. The activation energy of the oxidation of Si_3N_4 reported here (310 kJ/mol) is somewhat lower than values found in the literature, but of the same size as the one determined for Si_2N_2O (245 kJ/mol). This suggests that the same oxidation mechanism is valid in both cases. Furthermore, it indicates that the occurrence of minor amounts of Si_2N_2O in the oxide scale will not seriously impede the reaction. The

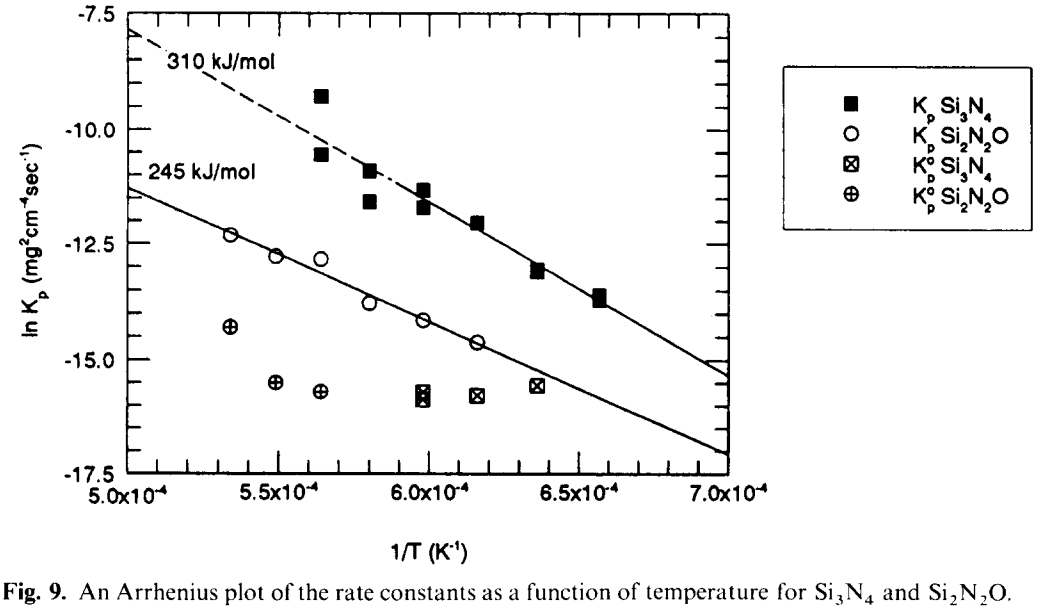

Fig. 9. An Arrhenius plot of the rate constants as a function of temperature for Si_3N_4 and Si_2N_2O.

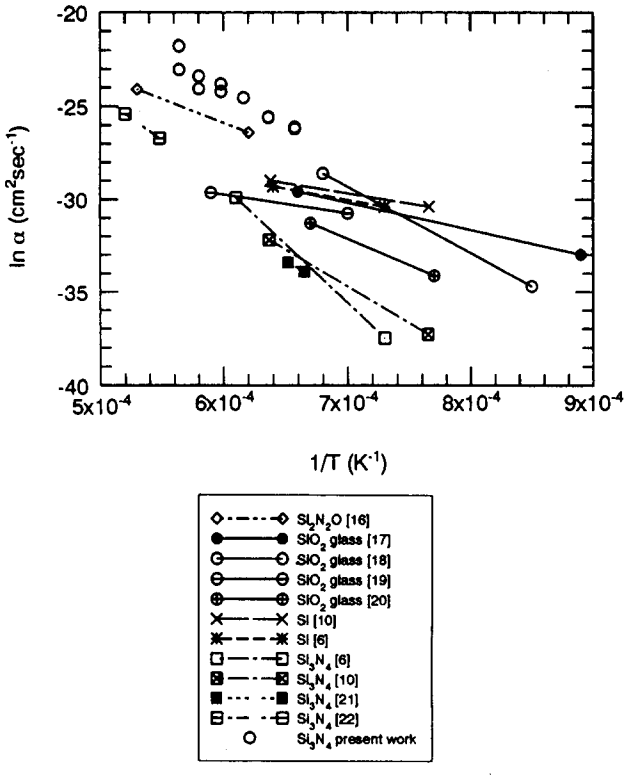

Fig. 10. An Arrhenius plot of α-values of Si_3N_4, Si, Si_2N_2O and the oxygen diffusion coefficients in fused silica (solid lines) measured by the isotope exchange method, together with the α-values determined in this report. The α-values found in the literature have been determined for Si_3N_4, prepared by chemical vapour deposition, and for single crystals of Si. The K_p values found in Ref. 22 have here been converted to α values using eqn (9).

activation energies we have determined by using the new rate law are within the range of those reported for the oxygen diffusion through amorphous silica.

Concluding remark

The obtained oxidation curves for Si_3N_4 are non-parabolic at 1250°C for 20 h and for the first 5–10 h at 1300 to 1500°C. These parts can, however, be described by the new rate law. The rate constants we have obtained by using the new rate law seem to be consistent among themselves, which means that this function could preferentially be used to calculate oxidation rates when crystallization or other effects cause a decrease of the cross-sectional area for oxygen diffusion.

Acknowledgement

This work has been financially supported by the Swedish Board for Industrial and Technical Development.

References

1. Singhal, S. C., Thermodynamics and kinetics of oxidation of hot-pressed silicon nitride. *J. Mat. Sci.*, **11** (1976) 500–509.
2. Tripp, W. C. & Graham, H. C., Oxidation of Si_3N_4 in the range 1300°C to 1500°C. *J. Am. Ceram. Soc.*, **59** (1976) 399–403.
3. Cubicciotti, D. & Lau, K. H., Kinetics of oxidation of yttria hot-pressed silicon nitride. *J. Electrochem. Soc.*, **126** (1979) 1723–8.
4. Clarke, D. R. & Lange, F. F., Oxidation of Si_3N_4 alloys: relation to phase equilibria in the system Si_3N_4–SiO_2–MgO. *J. Am. Ceram. Soc.*, **63** (1980) 586–93.
5. Babini, G. N., Bellosi, A. & Vincenzini, P., A diffusion model for the oxidation of hot-pressed Si_3N_4–Y_2O_3–SiO_2 materials. *J. Mat. Sci.*, **19** (1984) 1029–42.
6. Du, H., Tressler, R. E., Spear, K. E. & Pantano, C. G., Oxidation studies of crystalline CVD silicon nitride. *J. Electrochem. Soc.*, **136** (1989) 1527–35.
7. Zheng, Z., Tressler, R. E. & Spear, K. E., Oxidation of single-crystal silicon carbide. Part II. Kinetic model. *J. Electrochem. Soc.*, **137** (1990) 2812–16.
8. Costello, J. A. & Tressler, R. E., Oxidation kinetics of silicon carbide crystals and ceramics: I. In dry oxygen. *J. Am. Ceram. Soc.*, **69** (1986) 674–81.
9. Narushima, T., Goto, T. & Hirai, T., High-temperature passive oxidation of chemically vapor deposited silicon carbide. *J. Am. Ceram. Soc.*, **72** (1989) 1386–90.
10. Choi, D. J., Fischbach, D. B. & Scott, W. D., Oxidation of chemically-vapor-deposited silicon nitride and single-crystal silicon. *J. Am. Ceram. Soc.*, **72** (1989) 1118–23.
11. Nickel, K. G., Danzer, R., Schneider, G. & Petzow, G., Corrosion and oxidation of advanced ceramics. *Pow. Met. Int.*, **21** (1989) 29–33.
12. Echeberria, J. & Castro, F., Comparison between continuous and cyclic oxidation of fully dense Si_3N_4 + 1 w/o Y_2O_3. Structural ceramics—processing, microstructure and properties. In *Proc. 11th Risö Int. Symp. on Metallurgy and Materials Science*, ed. J. J. Bentzen *et al.* Roskilde, Denmark, 1990, pp. 249–55.
13. Persson, J., Ekström, T., Käll, P.-O. & Nygren, M., Oxidation behaviour and mechanical properties of β- and mixed α-β-sialons sintered with additions of Y_2O_3 and Nd_2O_3. *J. Eur. Ceram. Soc.* **11** (1993) 363–73.
14. Brodsky, M. B. & Cubicciotti, D., The oxidation of silicon at high temperatures. *J. Am. Ceram. Soc.*, **73** (1951) 3497–9.
15. Frisch, B., Thiele, W.-R., Drumm, R. & Münnich, B., On the oxidation mechanisms of silicon carbide in the 300°C to 1300°C temperature range. *Ber. DKG.*, **65** (1988) 277–84.
16. Persson, J., Käll, P.-O. & Nygren, M., Interpretation of the parabolic and non-parabolic oxidation behaviour of Si_2N_2O. *J. Am. Ceram. Soc.*, **75** (1992) 3377–84.
17. Williams, E. L., Diffusion of oxygen in fused silica. *J. Am. Ceram. Soc.*, **48** (1965) 190–4.
18. Sucov, E. W., Diffusion of oxygen in vitreous silica. *J. Am. Ceram. Soc.*, **46** (1963) 14–20.
19. Muchlenbachs, K. & Schaeffer, H. A., Oxygen diffusion in vitreous silica—utilization of natural isotopic abundance. *Can. Min.*, **15** (1977) 179–84.
20. Haul, R. & Dümbgem, G., Untersuchung der Sauerstoff-beweglichkeit in Titandioxyd, Quarz and Quarzglas mit Hilfe des heterogenen Isotopenaustausches. *Zeit. für Electrochemie*, **66** (1962) 636–41.
21. Fränz, I. & Langheinrich, W., Conversion of silicon nitride into silicon dioxide through the influence of oxygen. *Solid-State Elec.*, **14** (1971) 499–505.
22. Hirai, T., Niihara, K. & Goto, T., Oxidation of CVD Si_3N_4 at 1550°C to 1650°C. *J. Am. Ceram. Soc.*, **63** (1980) 419–24.